Published in final edited form as:
Int J Radiat Oncol Biol Phys. 2010 April ; 76(5): 1537–1545. doi:10.1016/j.ijrobp.2009.12.010.

Improved intratumoral oxygenation through vascular normalization increases glioma sensitivity to ionizing radiation

Mackenzie C. McGee, M.D.[1], **J. Blair Hamner, M.D.**[1,5], **Regan F. Williams, M.D.**[1,5], **Shannon F. Rosati, M.D.**[1], **Thomas L. Sims, M.D.**[1,5], **Catherine Y. Ng, M.S.**[1], **M. Waleed Gaber, Ph.D.**[7], **Christopher Calabrese, Ph.D.**[4], **Jianrong Wu, Ph.D.**[2], **Amit C. Nathwani, M.D., Ph.D**[8], **Christopher Duntsch, M.D., Ph.D.**[6], **Thomas E. Merchant, D.O., Ph.D.**[3], and **Andrew M. Davidoff, M.D.**[1,5]

[1]Department of Surgery, St. Jude Children's Research Hospital, Memphis, TN, USA

[2]Department of Biostatistics, St. Jude Children's Research Hospital, Memphis, TN, USA

[3]Department of Radiological Sciences, St. Jude Children's Research Hospital, Memphis, TN, USA

[4]The Animal Imaging Center, St. Jude Children's Research Hospital, Memphis, TN, USA

[5]Department of Surgery, University of Tennessee Health Science Center, Memphis, TN, USA

[6]Department of Neurosurgery, University of Tennessee Health Science Center, Memphis, TN, USA

[7]Department of Biomedical Engineering, University of Tennessee Health Science Center, Memphis, TN, USA

[8]Department of Hematology/Oncology, University College London, London, United Kingdom

Abstract

Purpose—Ionizing radiation, an important component of glioma therapy, is critically dependent on tumor oxygenation. However, gliomas are notable for areas of necrosis and hypoxia, which foster radioresistance. We hypothesized that pharmacologic manipulation of the typically dysfunctional tumor vasculature would improve intratumoral oxygenation and, therefore, the anti-glioma efficacy of ionizing radiation.

Methods and Materials—Orthotopic U87 xenografts were treated with either continuous interferon-beta (IFN-β) or bevacizumab, alone, or in combination with cranial irradiation (RT). Tumor growth was assessed by quantitative bioluminescence imaging; tumor vasculature, with immunohistochemical staining; and tumor oxygenation, with hypoxyprobe staining.

Results—Both IFN-β and bevaziumab profoundly affected the tumor vasculature, albeit with different cellular phenotypes. IFN-β caused a doubling in the percent area of perivascular cell staining while bevacizumab caused a rapid decrease in the percent area of endothelial cell staining. However, both agents increased intratumoral oxygenation, although with bevacizumab the effect was transient, being lost by five days. Administration of IFN-β or bevacizumab prior to RT was significantly more

Correspondence to: Andrew M. Davidoff, MD, Department of Surgery, St. Jude Children's Research Hospital, 262 Danny Thomas Place, Memphis, Tennessee 38105-3678. (901) 595-4060, fax: (901) 595-6621. (andrew.davidoff@stjude.org).

This work was presented, in part, at the 93rd annual meeting of the Radiological Society of North America on November 29, 2007.

Conflict of Interest Notification: Potential or actual conflicts of interests do not exist for any of the authors.

effective than any of the three modalities as monotherapy or when RT was administered concomitantly with IFN-β or bevacizumab, or five days after bevacizumab.

Conclusions—Bevacizumab and continuous delivery of IFN-β each induced significant changes in glioma vascular physiology, improving intratumoral oxygenation and enhancing the anti-tumor activity of ionizing radiation. Further investigation into the use and timing of these and other agents that modify vascular phenotype, in combination with radiation, is warranted in order to optimize cytotoxic activity.

Keywords

Vascular normalization; oxygenation; bevacizumab; interferon-beta; ionizing radiation; glioma

Introduction

High-grade gliomas are highly vascular, aggressive tumors with nearly universally fatal outcomes despite intensive multi-modality therapy that includes surgery, radiation and chemotherapy (1,2). The aggressive nature of high grade gliomas appears to be tied to the degree of angiogenesis (3,4). These tumors have been shown to express increased levels of a variety of angiogenic factors, including vascular endothelial growth factor (VEGF) (5-7), a cytokine known to play a critical role in the angiogenic phenotype of these and other solid tumors (8,9). However, VEGF promotes not only increased activation of endothelial cells but also increased vascular permeability. The resultant tumor vasculature is highly abnormal with vessels being leaky and generally very inefficient, leading to heterogeneous perfusion of the tumors (10). Therefore, tumors often have areas of hypoxia and low pH (11-13), which interfere with the cytotoxic effects of ionizing radiation (14,15) and promote resistance to radiation (16,17). Ionizing radiation kills tumor cells through a number of mechanisms including the generation of reactive oxygen species that damage DNA and interact with the cell membrane to trigger apoptosis. Therefore, achieving the same level of tumor cell killing requires three times the radiation dose under hypoxic conditions compared to normoxic states (18).

Chronically hypoxic tumors, including high-grade gliomas, pose significant clinical challenges and are more resistant to therapy. As they adapt to their conditions, hypoxic tumors become more genomically unstable and resistant to apoptosis (19). Measures to increase perfusion and oxygenation of tumors should theoretically increase cell death in response to radiation therapy. One way to improve intratumoral oxygenation may be through the normalization of the generally immature intratumoral vasculature. The concept of “vascular normalization” describes the effect of angiogenesis inhibitors on tumor vasculature in which there is at least a partial correction of the dysfunctional intratumoral vascular phenotype leading to improvement in tumor perfusion and oxygenation (20-22). This effect may only be transient, however, providing a limited window of opportunity to improve the anti-tumor activity of cytotoxic therapies that depend on tumor oxygenation and perfusion (23-25).

We have previously described two different methods that effect vascular normalization: one is through the continuous delivery of IFN-β; the other is through the administration of the anti-VEGF antibody, bevacizumab. We found that continuous, systemic IFN-β delivery, established with liver-targeted adeno-associated virus vectors (AAV-IFN-β), leads to sustained morphologic and functional changes of the tumor vasculature that are consistent with vessel maturation (26). These changes include increased smooth muscle cell coverage of tumor vessels and improved intratumoral blood flow, as well as decreased vessel permeability, tumor interstitial pressure, and intratumoral hypoxia (26). We have also found that bevacizumab, a recombinant monoclonal antibody against human VEGF, can also achieve vascular normalization, albeit through a different mechanism (27,28). Bevacizumab is currently being

used in a number of clinical trials in conjunction with chemotherapy and ionizing radiation, with promising preliminary results in a number of different tumor types, including brain tumors (29,30). Unlike continuous delivery of IFN-β, however, bevacizumab appears to achieve only transient normalization of the intratumoral vasculature. In the current study, we examined the ability of these two agents to improve intratumoral oxygenation and increase the efficacy of ionizing radiation in a murine glioma xenograft model. We also hypothesized that the timing of the administration of these two agents, relative to the delivery of ionizing radiation, would be critical for optimizing the anti-tumor effect of these treatments.

Methods and Materials

Vector production

Construction of the pAV2 CAG hIFN-β vector plasmid has been described previously (31). The hIFN-β vector plasmid includes the CMV-IE enhancer, β-actin promoter, a chicken β-actin/rabbit β-globin composite intron and a rabbit β globin polyadenylation signal (CAG) mediating the expression of the cDNA for human IFN-β. The expression cassette is flanked by the AAV-2 inverted terminal repeats (ITR). The cDNA's for hIFN-β and human placental alkaline phosphatase were purchased from InvivoGen (San Diego, CA). Recombinant AAV vectors pseudotyped with serotype 8 capsid were generated by transient transfection of 293T cells using the vector plasmid, a second plasmid, pAAV8-2 (32) from Dr. J. Wilson (Philadelphia, PA), for packaging and a third plasmid, pHGTI-adeno1, to provide adenoviral helper function. The AAV-2/8 vectors were purified using an ion exchange chromatography method (33). Standard quantitative PCR analysis was used to determine the vector particle titer. The vector stocks were consistently free of contamination with wt AAV and cellular and adenoviral proteins as judged by our previously described methods (26,31,32,34).

Animal model

All animal experiments were carried out in 4-6 week old, male CB-17 SCID mice (Charles' River Laboratories, Wilmington, MA). U87 cells expressing the firefly luciferase enzyme were generously provided by Dr. Robert Carter (Boston, MA). Intracranial tumors were established by first administering anesthesia with a mixture of ketamine (40μg/mg) and xylazine (40μg/mg). Mice were then placed on a stereotactic frame and after having their heads shaved, a 3 × 2 mm burr hole was made in the skull to expose the underlying dura mater using an M844 surgical microscope system (Leica Microsystems Inc, Allendale, NJ). U87-luciferase cells (5×10^5) were implanted in a volume of 10μL of sterile saline 3 mm deep to the brain surface over 5 minutes. Adhesive glue was used to close the defect in the skull. All animal studies were performed in accordance with an institutional IACUC approved protocol.

Real time assessment of tumor burden was performed with bioluminescence imaging using an IVIS Imaging System 100 Series (Xenogen Corporation, Alameda, CA) as we, and others, have previously shown that bioluminescence signal correlates with tumor burden (35,36). An intraperitoneal injection of D-luciferin (Xenogen) at 15 mg per mL in sterile saline was administered to mice. Five minutes later, mice were imaged at a distance of 25cm from the light detector. Images were analyzed with Living Image Software version 2.50 (Xenogen). Bioluminescence was recorded as photons per second. Tumor size at the time of sacrifice was measured directly from hematoxylin and eosin stained brain sections to confirm that the bioluminescence signal accurately reflected tumor burden. Tumors were measured in two directions with volume calculated as (length × width^2)/2.

Mice treated with bevacizumab (Genentech, San Francisco, CA) received a single intravenous injection of 200μg. Mice were sacrificed on days 0 (1 hr after administration of bevacizumab), two and five with harvested tissue then analyzed for CD34 and pimonidazole staining. Mice

treated with IFN-β received 1.5×10^{10} vector particles of AAV2/8 CAG hIFN-β in a volume of 200 μl of PBS by tail vein injection. Systemic levels of IFN-β in mouse plasma were measured using commercially available immunoassays (ELISA, Fujirebio Inc, Tokyo, Japan). Mice that received radiation therapy were anesthetized with a ketamine and xylazine mixture and a single dose of 10 Gy was delivered to the head, with body shielding, using a D3300 Gulmay orthovoltage treatment system (Gulmay Medical Ltd, England, UK) at a dose rate of 0.76 Gy/minute.

Immunohistochemistry and immunofluorescence

Formalin fixed, paraffin embedded 4μm thick tumor sections were analyzed by immunohistochemical (IHC) staining for endothelial cells using a rat anti-mouse CD34 (RAM 34, PharMingen, San Diego, CA) antibody and for perivascular cells using a mouse anti-human smooth muscle actin (clone 1A4, DAKO, Carpenteria, CA) antibody. Immunofluorescence staining was conducted on formalin-fixed, paraffin-embedded tumor samples with a rat anti-mouse CD34 antibody (eBioscience, 14-0341-85, San Diego, CA) and a mouse anti-human smooth muscle actin (SMA, DAKO M0851, Clone 1A4, Carpenteria, CA). Secondary antibodies were goat anti-rat Alexa Fluor 647 and goat anti-mouse Alexa Fluor 555 (Invitrogen). Intratumoral hypoxia was assessed using a commercially available Hypoxyprobe™-1 kit for the detection of tissue hypoxia (Chemicon International, Temecula, CA). Pimonidazole hydrochloride was given at a dose of 60 mg/kg in 0.9% saline via intraperitoneal injection one hour before euthanasia, and orthotopic tumors were harvested and fixed in formalin. As hypoxia may vary with tumor size, size-matched controls were used for comparison. H&E and IHC stained sections were viewed and digitally photographed using an Olympus U-SPT microscope equipped with both fluorescence and bright field illumination with an attached CCD camera. Three images at 20X magnification were captured for each tumor sample concentrating on well-vascularized, non-necrotic regions and were saved as JPEG files for further processing in Adobe Photoshop (Adobe Systems Incorporated, San Jose, CA). Light and camera gain were not changed between capturing images for each set of slides. Positive staining was highlighted by eliminating other colors with the magic wand tool at a tolerance of 60 pixels in Adobe Photoshop (San Jose, CA). Once only brown color was left in the picture, the picture was gray scaled and then made monochrome using a 50% threshold. The monochrome bitmap image was then analyzed for pixels using the NIH analysis software, ImageJ. Data are presented as percent positive stained area. The percentage of co-localization of CD34 and αSMA was calculated by determining the percentage of CD34-positive cells that had αSMA-positive cells immediately adjacent to them, in the original JPEG images.

Statistical analysis

Continuous variables are reported as mean ± standard error of the mean (SEM) and were compared using an unpaired Student's t-test. Bliss's independent joint action principle was used to define a synergy index (SI) with 95% confidence intervals being used to assess drug interaction (37). A SI less than 1 with a 95% confidence interval that does not cross zero suggests synergy of two therapies. A p value of less than 0.05 was considered significant. Data was analyzed and graphed using SigmaPlot (Version 9, SPSS, Inc, Chicago, IL).

Results

Alteration of the intratumoral vasculature and oxygenation with continuous IFN-β

Two weeks after U87 tumor cell inoculation, intracranial tumors were size-matched based on bioluminescence, and one cohort (n=4) was treated with AAV-IFN-β. Mice were sacrificed after 14 days of therapy, and tumors harvested for immunohistochemical analysis. Consistent with the effect previously reported in a subcutaneous model (25), treatment with continuous IFN-β increased vascular smooth muscle coverage of intratumoral blood vessels (Figure 1A).

Quantitative image analysis revealed a significant increase in SMA staining in treated intracranial ($p<0.001$) tumors compared to controls (n=4, Figure 1A). IFN-β also decreased the percent area of endothelial cell stained cells (0.2±0.05% CD34 positive area vs 0.7±0.09% CD34 positive area, $p = 0.009$). To confirm that SMA stained cells represented perivascular cells, immunofluorescence was used to co-localize the SMA stained cells with the endothelial cells with a significant increase in co-localization being observed in IFN treated tumor samples (13.8±7.4 vs 56.1±9% CD34 cells co-localized with SMA cells, p=0.01, Figure 1B).

To confirm that this change in vessel cellular morphology would improve intratumoral oxygenation, tumor hypoxia was evaluated in these same cohorts of mice with hypoxyprobe immunohistochemical staining. Treatment with IFN-β resulted in significantly decreased intratumoral hypoxia staining (Figure 2A). When images were analyzed using ImageJ, IFN-β treatment resulted in a 97.5% (p=0.002) reduction in hypoxia in orthotopic tumors (Figure 2B), although the smaller size of IFN-β treated tumors may have contributed somewhat to the decreased hypoxia.

Alteration of the intratumoral vasculature and oxygenation with bevacizumab

After establishment of intracranial tumors, mice were treated with a single dose of bevacizumab, and tumor tissue was analyzed at day 0, 2 and 5 for changes in vasculature and oxygenation. Two days after bevacizumab administration, the number of CD34-positive cells in treated tumors decreased by 32% (n=15, p=0.084); this decrease reached statistical significance five days following treatment (n=12, p=0.00022, Fig 3A). Bevacizumab had no effect on the percent area of perivascular-stained cells (data not shown).

Tumor hypoxia was quantified by immunohistochemical analysis of intracranial tumor sections (Figure 3B). A significant improvement in tumor oxygenation (200%) was observed in bevacizumab-treated tumors at two days compared with matched control tumors (p=0.028, Figure 3B). This effect was transient, however, as five days after therapy, intratumoral hypoxia returned to control values (p=0.50).

Xenograft growth inhibition with continuous IFN-β and RT treatment

Ten days after tumor cell inoculation, the presence of established intracranial tumors was confirmed by bioluminescence imaging. The effect of treatment on tumor burden was then followed by serial bioluminescent imaging. Although we have previously shown that tumor bioluminescence may overestimate size somewhat if there is a concomitant improvement in tumor perfusion (26), in this current study tumor burden based on bioluminescence accurately reflected relative tumor volumes based on direct tumor measurement at the time of sacrifice and magnetic-resonance imaging (MRI, Figure 4). Mean bioluminescent signal prior to treatment was $2.91\times10^7\pm4.4\times10^6$ photons/sec. Mice were then size-matched by bioluminescent signal intensity into 2 cohorts. The cohort treated with IFN-β alone had lower mean bioluminescent signals compared to controls 7 and 14 days after administration of AAV-IFN-β (Figure 4). These differences were statistically significant at Day 14 based on bioluminescence ($2.84\times10^8\pm5.39\times10^7$ photons/sec vs. $4.44\times10^7\pm1.36\times10^{7;}$ p=0.003) and direct tumor measurements (8.32±2.7 mm^3 vs. 0.91±0.49 mm^3, p=0.03). The mean plasma level of IFN-β in the treated groups was 80±10 ng/ml at Day 14.

In another experiment, U87 xenografts with a mean bioluminescence signal of $2.42\times10^7\pm 3.59\times10^6$ photons/sec were divided into four cohorts. One cohort received AAV-IFN-β only, one received intracranial radiation (10Gy) only, one cohort was untreated, and one cohort received intracranial radiation (10 Gy) 5 days following administration of AAV-IFN-β. Those treated with AAV-IFN-β ($2.47\times10^8\pm5.02\times10^7$photons/sec, p=0.001) or RT ($3.93\times10^8\pm5.34\times10^7$photons/sec, p=0.02) had significantly lower mean bioluminescence

signals compared to controls ($5.78\times10^8\pm3.07\times10^7$photons/sec) two weeks after treatment. The combination of AAV-IFN-β followed by RT resulted in a mean bioluminescence signal of $4.40\times10^7\pm2.32\times10^6$photons/sec two weeks after initial therapy. This was significantly lower than the observed signal after both AAV-IFN-β (p=0.02) and RT (p=0.004) monotherapies. The final signal in the combined treatment group was not significantly different from the baseline, pre-treatment signal (Figure 5A). The combination of IFN-β and XRT was synergistic based on a SI of -1.339±0.583 (-2.482, -0.196).

Simultaneous treatment with AAV-IFN-β and RT was then compared to treatment with AAV-IFN-β followed by RT five days later. Mice with tumors treated with RT 5 days after administration of AAV-IFN-β had significantly less tumor burden than mice treated with RT and AAV-IFN-β simultaneously ($3.25\times10^7\pm4.6\times10^6$ photons/sec, n=5 vs $1.53\times10^8\pm5.3\times10^7$ photons/sec, n=5, p = 0.04, Figure 5B). This result suggests that the synergistic effect of IFN-β and RT may be secondary to improved tumor oxygenation.

Xenograft growth inhibition with bevacizumab and RT treatment

Cohorts of tumor-bearing mice were first treated with bevacizumab or radiation alone to determine the effect of monotherapy. Additional cohorts of mice with established U87 xenografts were treated with bevacizumab followed by 10 Gy of intracranial radiation at day 0, 2 or 5. Tumor growth was assessed by bioluminescent imaging 14 days after treatment with bevacizumab prior to harvesting tissue for histologic evaluation. Inhibition of intracranial xenografts was greatest when RT was given 2 days after bevacizumab ($1.64\times10^8\pm7.08\times10^7$ photons/sec, n=9) when compared to controls ($1.10\times10^9\pm3.63\times10^8$ photons/sec, n=10, p=0.02), bevacizumab alone ($6.56\times10^8\pm1.42\times10^8$ photons/sec, n=4, p=0.005), RT alone ($8.38\times10^8\pm2.60\times10^8$ photons/sec, n=4, p=0.005), bevacizumab followed immediately by RT ($4.93\times10^8\pm1.78\times10^7$ photons/sec, n=7, p=0.08), and bevacizumab followed by RT 5 days later (3.89×10^8 photons/sec$\pm5.82\times10^7$, n=9, p=0.03) (Figure 6). When assessing for synergy among combination groups, only the combination of administering radiation 2 days after a single dose of bevaciumab was synergistic based on a SI of -1.429±0.631 (-2.667, -0.1915). The combination of radiation given simultaneously with bevacizumab or five days following bevacizumab was considered additive based on a SI of -0.333±0.587 (-1.484, 0.818) and -0.568 ±0.486 (-1.521, 0.385), respectively. Thus, in this orthotopic model, timing of radiation two days after a single dose of bevacizumab showed the greatest effect on tumor growth.

Discussion

Clinical outcomes for patients with high-grade glioma remain poor despite increased intensity of multi-modality therapy. We investigated the therapeutic benefit of combining anti-angiogenic agents with ionizing radiation in a relevant glioma model to test the hypothesis that vascular normalization and resultant increased tumor oxygenation would improve glioma sensitivity to ionizing radiation.

We have previously shown, in a variety of tumor models, that AAV-mediated delivery of IFN-β has significant anti-tumor efficacy (26,31,32,34,38). In addition, we have demonstrated in a murine model of neuroblastoma that AAV-IFN-β effects improved pericyte coverage of tumor blood vessels, and decreased branching and tortuosity of the tumor vasculature (26,38). These changes, in turn, altered intratumoral vascular physiology by lowering interstitial fluid pressure, reducing vessel permeability, and decreasing intratumoral hypoxia (26). Thus, IFN-β effected “normalization” of the tumor vasculature.

In this study we have demonstrated that this method of delivering IFN-β is efficacious in restricting tumor progression in an orthotopic xenograft model of glioma. In addition, IFN-β again produced significant morphologic and physiologic changes in the tumor vasculature, and

effected a significant improvement in intratumoral oxygenation in intracranial xenografts. These changes created a microenvironment within the tumor that appeared to be, at least partly, responsible for the radiosensitizing effects of IFN-β. We theorize that it is the increase in tumor oxygenation that enhances the antitumor effect of ionizing radiation, as previous results in vitro have shown that there is a lack of direct radiosensitization by recombinant IFN-β in several glioma cell lines, including U87 (39). The combination of IFN-β and radiation was synergistic supporting the hypothesis that IFN-β has radiosensitizing effects as well as cytotoxic effects. Although systemic delivery of IFN-β may not ultimately be practical clinically, local gene transfer to establish a local milieu of continuous IFN-β may be an alternative approach.

We have also previously shown that bevacizumab-mediated VEGF blockade effects alterations in tumor vessel physiology that result in improved vascular function and allow for more efficient delivery and efficacy of systemically administered chemotherapy, although careful consideration of drug scheduling was required to optimize antitumor activity (28). In our current study, bevacizumab again effected intratumoral vascular normalization, this time in intracranial glioma xenografts, and there again appeared to be an optimal schedule for the dosing of adjuvant therapy (RT) when used in combination with bevacizumab because of the transient normalization of the tumor vasculature. Bevacizumab caused a prolonged decrease in the mean intratumoral vessel density, consistent with prior reports (24). However, despite this, there was transient improvement in intratumoral oxygenation, consistent with vascular normalization, which correlated with anti-tumor activity. Bevacizumab given two days prior to RT, versus five days prior to RT, was the most effective treatment regimen in an intracranial model and was synergistic. This correlated with changes in tumor oxygenation allowing for more effective radiation therapy.

In a similar study, Winkler et al. showed previously that VEGFR2 blockade created a normalization window characterized by increased tumor oxygenation, increased pericyte coverage of brain tumor vessels, and improved response to RT (25). Similarly, Dings et al. recently reported that RT delivery is most effective during a “tumor oxygenation window” which they show exists up to four days following treatment with bevacizumab in heterotopic models of human ovarian carcinoma, and murine melanoma and breast carcinoma (24). In our study, we evaluated glioma xenografts, a tumor type with a treatment approach that typically includes RT, and used an orthotopic (intracranial) model. There was a significant decrease in intratumoral hypoxia two days following bevacizumab as measured by pimonidazole staining, with a return towards control measurements five days following treatment. The timing of maximal improvement in tumor oxygenation secondary to bevacizumab directly coincided with maximum anti-tumor effects of combined therapy with RT, suggesting that improved tumor oxygenation plays a significant role in glioma response to bevacizumab and RT combination therapy.

Thus, in this study we have shown that improved intratumoral oxygenation, caused by agents that effect normalization of the vasculature through different mechanisms, can improve the anti-glioma activity of RT. Our study also suggests, however, that the timing of delivery of vasculature-modifying agents in relation to RT is important because this effect may be transient. Therefore, although these combinations are effective, further investigation into the use and timing of these and other anti-angiogenic agents when used in combination with ionizing radiation is warranted in order to optimize cytotoxic activity.

Acknowledgments

Grant Support: This work was supported by the Assisi Foundation of Memphis, the US Public Health Service Childhood Solid Tumor Program Project Grant No. CA23099, the Cancer Center Support Grant No. 21766 from the National Cancer Institute, and by the American Lebanese Syrian Associated Charities (ALSAC).

References

1. Stupp R, Mason WP, van den Bent MJ, et al. Radiotherapy plus concomitant and adjuvant temozolomide for glioblastoma. N Engl J Med 2005;10:987–996. [PubMed: 15758009]
2. Wrensch M, Minn Y, Chew T, et al. Epidemiology of primary brain tumors: current concepts and review of the literature. Neurooncol 2002;4:278–99.
3. Fischer I, Gagner J, Newcomb E, Zagzag D. Angiogenesis in gliomas: biology and molecular pathophysiology. Brain Pathology 2005;15(4):297–310. [PubMed: 16389942]
4. Brown J, Giaccia A. The unique physiology of solid tumors: opportunities (and problems) for cancer therapy. Cancer Res 1998;58:2408–16.
5. Plate KH, Breier G, Weich HA, et al. Vascular endothelial growth factor is a potential tumour angiogenesis factor in human gliomas in vivo. Nature 1992;359:845–8. [PubMed: 1279432]
6. Plate KH, Breier G, Millauer B, et al. Up-regulation of vascular endothelial growth factor and its cognate receptors in a rat glioma model of tumor angiogenesis. Cancer Res 1993;53:5822–27. [PubMed: 7694795]
7. Salmaggi A, Eoli M, Frigerio S, et al. Intracavitary VEGF, bFGF, IL-8, IL-12 levels in primary and recurrent malignant glioma. J Neurooncol 2003;62:297–303. [PubMed: 12777082]
8. Ferrara N, Gerber HP, LeCouter J. The biology of VEGF and its receptors. Nat Med 2003;9:669–76. [PubMed: 12778165]
9. Hicklin DJ, Ellis LM. Role of the vascular endothelial growth factor pathway in tumor growth and angiogenesis. J Clin Oncol 2005;23:1011–27. [PubMed: 15585754]
10. Kaur B, Tan C, Bratt D, Post D, Van Meir E. Genetic and hypoxic regulation of angiogenesis in gliomas. J Neurooncol 2004;70(2):229–43. [PubMed: 15674480]
11. Cairns R, Papandreou I, Denko N. Overcoming physiologic barriers to cancer treatment by molecularly targeting the tumor microenvironment. Mol Cancer Res 2006;4:61–70. [PubMed: 16513837]
12. Carmeliet P, Jain RK. Angiogenesis in cancer and other diseases. Nature 2000;407:249–57. [PubMed: 11001068]
13. Fidler IJ, Ellis LM. Neoplastic angiogenesis—not all blood vessels are created equal. N Engl J Med 2004;351:215–6. [PubMed: 15254281]
14. Martinive P, De Wever J, Bouzin C, et al. Reversal of temporal and spatial heterogeneities in tumor perfusion identifies the tumor vascular tone as a tunable variable to improve drug delivery. Mol Cancer Ther 2006;5:1620–1627. [PubMed: 16818522]
15. Tannock IF. Tumor physiology and drug resistance. Cancer Metastasis Rev 2001;20:123–32. [PubMed: 11831640]
16. Mottram J. Factors of importance in radiosensitivity of tumors. Br J Radiol 1926;9:606.
17. Overgaard J, Horsman M. Modification of hypoxia induced radioresistance in tumors by the use of oxygen and sensitizers. Semin Radiat Oncol 1996;6:10–21. [PubMed: 10717158]
18. Overgaard J. Hypoxic radiosensitization: adored and ignored. J Clin Oncol 2007;25(26):4066–74. [PubMed: 17827455]
19. Rampling R, Cruickshank G, Lewis AD, et al. Direct measurement of pO2 distribution and bioreductive enzymes in human malignant brain tumors. Int J Radiat Oncol Biol Phys 1994;29:427–431. [PubMed: 8005794]
20. Jain RK. Normalizing tumor vasculature with anti-angiogenic therapy: a new paradigm for combination therapy. Nat Med 2001;7:987–9. [PubMed: 11533692]
21. Le Serve AW, Hellman K. Metastases and the normalization of tumour blood vessels by ICRF 159: a new type of drug action. Br Med J 1972;1:597–601. [PubMed: 4111169]
22. Teicher BA, Holden SA, Ara G, et al. Potentiation of cytotoxic cancer therapies by TNP-470 alone and with other anti-angiogenic agents. Int J Cancer 1994;57:920–5. [PubMed: 7515861]
23. Dings RP, Williams BW, Song CW, et al. Simultaneous inhibition of the receptor kinase activity of vascular endothelial, fibroblast, and platelet-derived growth factors suppresses tumor growth and enhances tumor radiation response. Cancer Res 2002;62:1702–1706. [PubMed: 11912143]

24. Dings RP, Loren M, Heun H, et al. Scheduling of Radiation with Angiogenesis Inhibitors Anginex and Avastin Improves Therapeutic Outcome via Vessel Normalization. Clin Cancer Res 2007;13:3395–3402. [PubMed: 17545548]
25. Winkler F, Kozin SV, Tong RT, et al. Kinetics of vascular normalization by VEGFR2 blockade governs brain tumor response to radiation: Role of oxygenation, angiopoietin-1, and matrix metalloproteinases. Cancer Cell 2004;6:553–562. [PubMed: 15607960]
26. Dickson P, Hamner J, Streck C, Ng C, McCarville M, Calabrese C, Gilbertson R, Stewart C, Wilson C, Gaber W, Pfeffer L, Skapek S, Nathwani A, Davidoff A. Continuous delivery of interferon beta promotes sustained maturation of intratumoral vasculature. Mol Cancer Res 2007;5(6):531–42. [PubMed: 17579115]
27. Gerber HP, Ferrara N. Pharmacology and pharmacodynamics of bevacizumab as monotherapy or in combination with cytotoxic therapy in preclinical studies. Cancer Res 2005;65:671–80. [PubMed: 15705858]
28. Dickson PV, Hamner JB, Sims TL, et al. Bevacizumab-induced transient remodeling of the vasculature in neuroblastoma xenografts results in improved delivery and efficacy of systemically administered chemotherapy. Clin Cancer Res 2007;13:3942–3950. [PubMed: 17606728]
29. Hurwtiz H, Fehrenbacher L, Novotny W, et al. Bevacizumab plus irinotecan, fluorouracil, and leucovorin for metastatic colorectal cancer. N Engl J Med 2004;(350):2335–42. [PubMed: 15175435]
30. Miller K, Wang M, Gralow J, et al. Paclitaxel plus bevacizumab versus paclitaxel alone for metastatic breast cancer. N Engl J Med 2007;357:2666–76. [PubMed: 18160686]
31. Streck C, Dickson P, Ng C, Zhou J, Gray J, Nathwani A, Davidoff A. Adeno-associated virus vector-mediated systemic delivery of interferon-beta combined with low-dose cyclophosphamide affects tumor regression in murine neuroblastoma models. Clin Cancer Res 2005;11(16):6020–29. [PubMed: 16115947]
32. Benjamin R, Kwaja A, Singh N, McIntosh J, Meager A, Madwha M, Streck C, Ng C, Davidoff A, Nathwani A. Continuous delivery of human type I interferons (alpha/beta) has significant activity against acute myeloid leukemia cells in vitro and in a xenografts model. Blood 2007;109(3):1244–7. [PubMed: 17047156]
33. Davidoff AM, Ng CY, Sleep S, Gray J, Azam S, Zhao Y, McIntosh JH, Karimipoor M, Nathwani AC. Purification of recombinant adeno-associated virus type 8 vectors by ion exchange chromatography generates clinical grade vector stock. J Virol Methods 2004 Nov;121(2):209–15. [PubMed: 15381358]
34. Streck C, Dickson P, Ng C, Zhou J, Hall M, Gray J, Nathwani A, Davidoff A. Antitumor efficacy of AAV-mediated systemic delivery of interferon-beta. Cancer Gene Ther 2006;13(1):99–106. [PubMed: 16052229]
35. Szentirmai O, Baker C, Lin N, Szucs S, Takahashi M, Kiryu S, Kung A, Mulligan R, Carter B. Noninvasive bioluminescence imaging of luciferase expressing intracranial U87 xenografts: correlation with magnetic resonance imaging determined tumor volume and longitudinal use in assessing tumor growth and antiangiogenic treatment effect. Neurosurgery 2006;58(2):365–72. [PubMed: 16462491]
36. Dickson PV, Ng CY, Zhou J, McCarville MB, Davidoff AM. In vivo bioluminescence imaging for early detection and monitoring of disease progression in murine model of neuroblastoma. J Pediatr Surg 2007;42(7):1172–1179. [PubMed: 17618876]
37. Plackett RL, Hewlett PS. Statistical aspects of the independent joint action of poisons, particularly insecticides; the toxicity of a mixture of poisons. Ann Appl Biol 1948 Sep;35(3):347–58. [PubMed: 18121530]
38. Dickson P, Hagedorn N, Hamner J, Fraga C, Ng C, Stewart C, Davidoff A. Interferon beta-mediated vessel stabilization improves delivery and efficacy of systemically administered topotecan in a murine neuroblastoma model. J Pediatr Surg 2007;42(1):160–5. [PubMed: 17208558]
39. Schmidberger H, Rave-Frank M, Lehmann J, Weiss E, Gerl L, Dettmer N, Glomme S, Hess C. Lack of interferon-beta induced radiosensitization in four out of five human glioblastoma cell lines. Int J Radiat Oncol Biol Phys 2003;55(5):1348–57. [PubMed: 12654447]

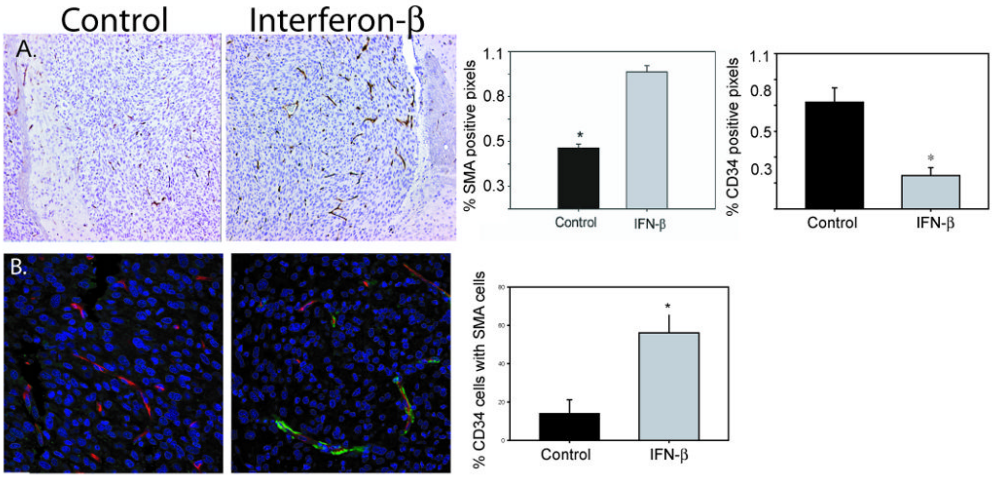

Figure 1. Continuous IFN-β increases smooth muscle coverage of tumor blood vessels

(A) α-SMA stained control and AAV-IFN-β treated tumors samples (20×) with bar graph quantifying the increase in pericytes ($p < 0.0001$) and a decrease in CD34 stained cells (endothelial cells), $p=0.009$. (B) Immunofluorescent co-stain for CD34 (red), α-SMA (green), and dapi (blue), 40×, with bar graph representing the percent of endothelial cells co-localized with α-SMA cells, $p = 0.01$. Data presented as mean +/-SEM.

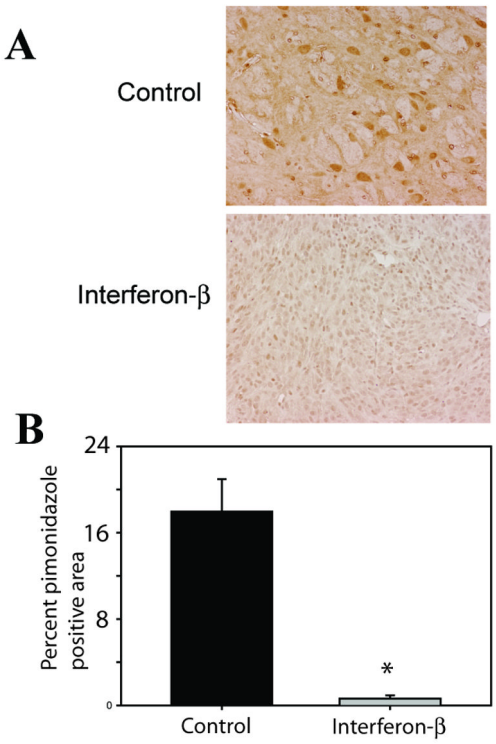

Figure 2. Continuous IFN-β decreases intratumoral hypoxia

In orthotopic glioma models, control tumors had significantly more hypoxic cells than IFN treated tumors (A). Quantitation with ImageJ software is also shown (B, *p<0.001). Data presented as mean +/- SEM.

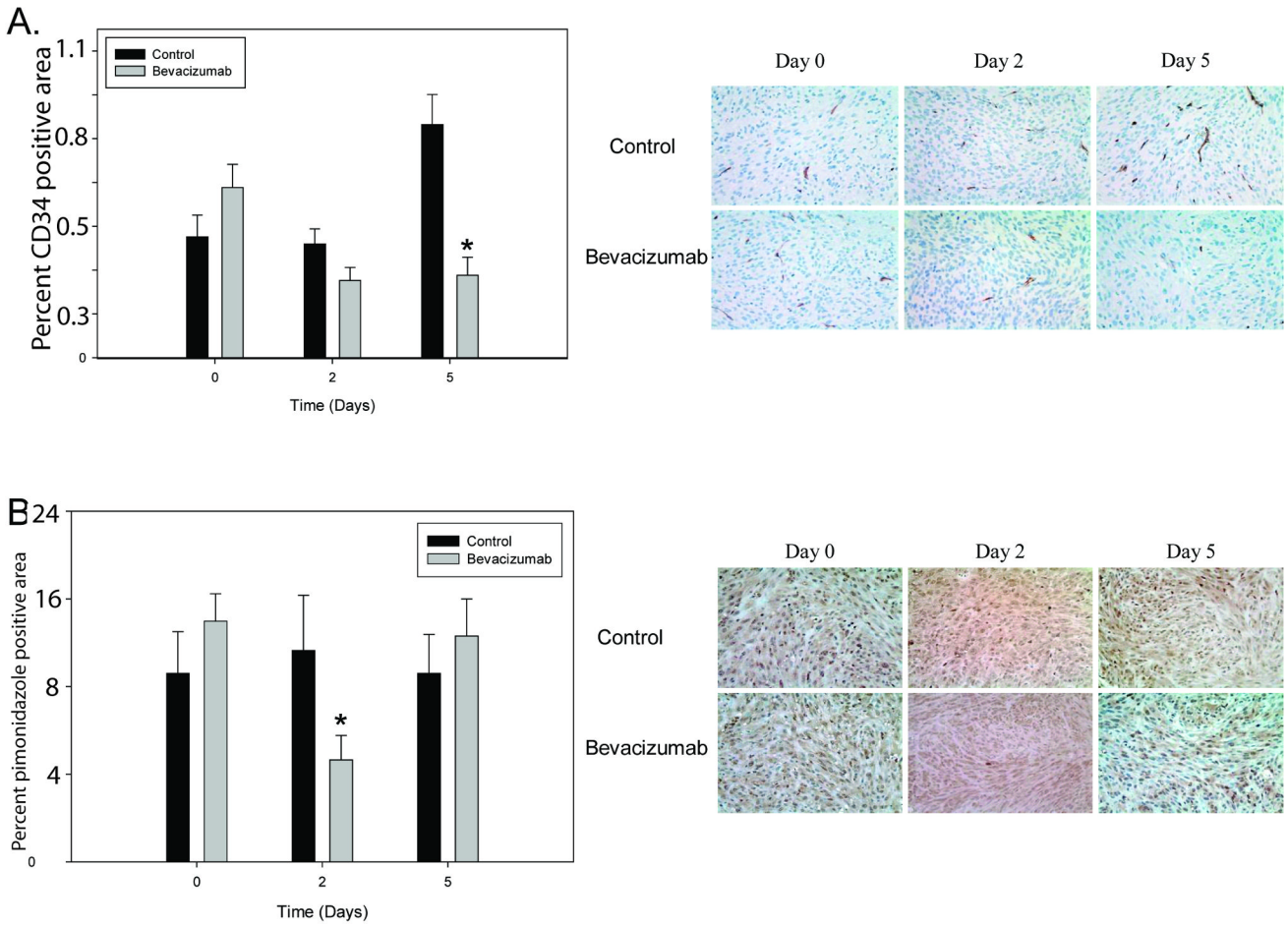

Figure 3. Changes in tumor vasculature with bevacizumab treatment

(A) In intracranial tumors, the decrease in percent vascular area in treated tumors was apparent two days following treatment (p=0.084) with a significant, sustained decrease present on day five (p=0.00022). Shown are representative sections stained with an anti-CD34 antibody (40×). **(B)** Decreased intratumoral hypoxia following treatment with bevacizumab compared to size-matched controls, as measured by pimonidazole staining with representative images shown (40×) at day 0 (p=0.29), day 2 (p=0.03), and day 5 (p=0.50) following single dose bevacizumab. *p<0.05, Data presented as mean +/- SEM.

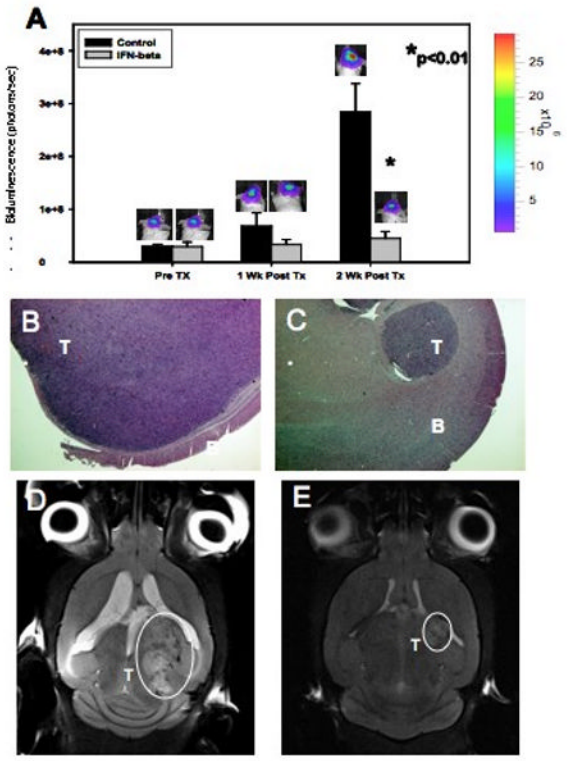

Figure 4. Continuous IFN-β restricts glioma progression in an orthotopic murine model

Human glioma xenografts show significant growth restriction two weeks after mice were treated with AAV IFN-β (A). Also shown are H&E stained sections (10×) of mice brains bearing control (B) and IFN-β-treated (C) tumors and MR images (D, E) after two weeks of therapy. T = tumor, B = brain. Data presented as mean +/- SEM.

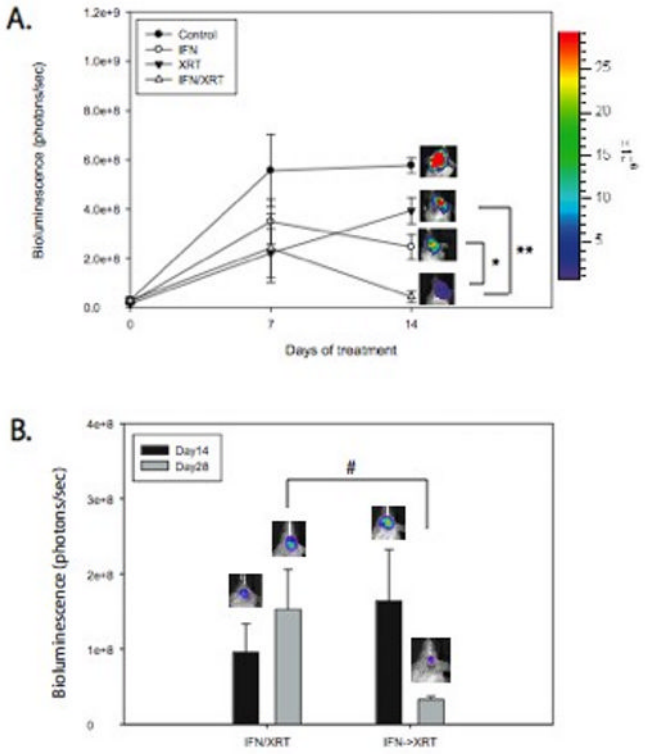

Figure 5. Treatment with continuous IFN-β prior to administering radiation therapy significantly improves the efficacy of radiation

While IFN and XRT are effective at restricting tumor growth, XRT five days following administration of IFN was significantly better than either monotherapy (A, *p=0.01 vs. IFN, **p=0.007 vs. XRT). When compared to simultaneous treatment with IFN and XRT, administering XRT 5 days after administration of IFN-β improved the antitumor effect of combination therapy (B, #p=0.04). Black=day 0, Gray=day 14 after initial therapy. Data presented as mean +/- SEM.

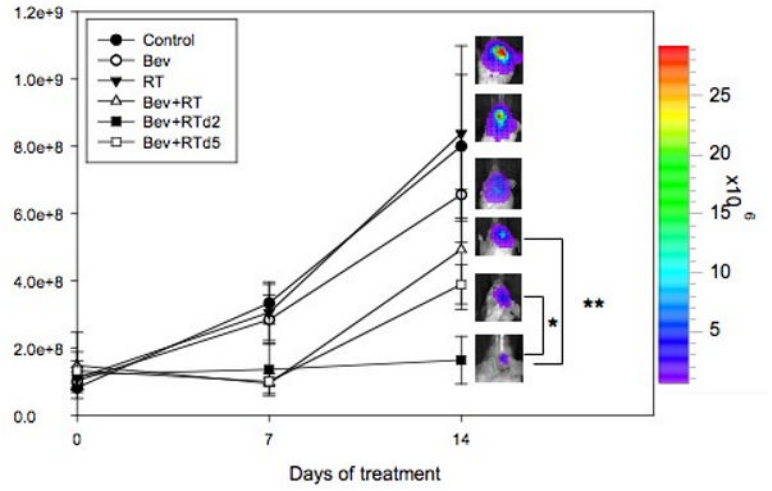

Figure 6. Treatment with bevacizumab prior to radiation therapy significantly improves the efficacy of radiation in tumors

Tumor burden in orthotopic, intracranial tumors 14 days following therapy as measured by bioluminescence imaging. Tumors treated with bevacizumab, with RT two days later (Bev+RT d.2) had greater reduction of tumor signal intensity as compared with tumors treated with bevacizumab and RT simultaneously (Bev+RT, *p=0.08) and RT five days after treatment with bevacizumab (Bev+RT d.5, **p=0.03). Data presented as mean +/- SEM.